

# Cloud-radiation-precipitation associations over the Asian monsoon region: an observational analysis

Jiandong Li<sup>1,2</sup> · Wei-Chyung Wang<sup>3</sup> · Xiquan Dong<sup>4,5</sup> · Jianguo Mao<sup>1</sup>

Received: 31 December 2015 / Accepted: 20 December 2016 / Published online: 13 January 2017  
© Springer-Verlag Berlin Heidelberg 2017

**Abstract** This study uses 2001–2014 satellite observations and reanalyses to investigate the seasonal characteristics of Cloud Radiative Effects (CREs) and their associations with cloud fraction (CF) and precipitation over the Asian monsoon region (AMR) covering Eastern China (EC) and South Asia (SA). The CREs exhibit strong seasonal variations but show distinctly different relationships with CFs and precipitation over the two regions. For EC, the CREs is dominated by shortwave (SW) cooling, with an annual mean value of  $-40 \text{ W m}^{-2}$  for net CRE, and peak in summer while the presence of extensive and opaque low-level clouds contributes to large Top-Of-Atmosphere (TOA) albedo ( $>0.5$ ) in winter. For SA, a weak net CRE exists throughout the year due to in-phase compensation of SWCRE by longwave (LW) CRE associated with the frequent occurrence of high clouds. For the entire AMR, SWCRE strongly correlates with the dominant types of CFs, although the cloud vertical structure plays important

role particularly in summer. The relationships between CREs and precipitation are stronger in SA than in EC, indicating the dominant effect of monsoon circulation in the former region. SWCRE over EC is only partly related to precipitation and shows distinctive regional variations. Further studies need to pay more attention to vertical distributions of cloud micro- and macro-physical properties, and associated precipitation systems over the AMR.

**Keywords** Cloud radiative effect · Cloud fraction · Precipitation · Asian monsoon region · Seasonal variation

## 1 Introduction

Clouds play key roles in energy and hydrological cycle of earth climate system by influencing atmospheric radiative heating, surface energy balance, general circulation and resulting precipitation (Randall et al. 2007; Boucher et al. 2013). In past decades, significant effort has been made to study the global distribution of cloud physical properties and their climate impacts using both satellite observations and climate model simulations (Trenberth et al. 2009; Stubenrauch et al. 2013), especially cloud radiative effects (CREs) (Loeb et al. 2009). The CREs at the top of the atmosphere (TOA) represent the bulk effects of clouds on shortwave (SW) and longwave (LW) radiation and are an effective method of studying cloud-radiation interactions and diagnosing relevant problems in climate models (Ramanathan et al. 1989; Loeb et al. 2012a, b). Precipitation is a key indicative of hydrological cycle. Thus, CREs have some potential physical relationships with precipitation through general circulation and cloud properties determining CREs. Currently, global schematic diagrams of global cloud-radiation balance have

✉ Jiandong Li  
lijd@mail.iap.ac.cn

<sup>1</sup> State Key Laboratory of Numerical Modeling for Atmospheric Sciences and Geophysical Fluid Dynamics (LASG), Institute of Atmospheric Physics, Chinese Academy of Sciences, P.O. Box 9804, Beijing 100029, China

<sup>2</sup> Collaborative Innovation Center on Forecast and Evaluation of Meteorological Disasters, Nanjing University of Information Science and Technology, Nanjing 210044, China

<sup>3</sup> Atmospheric Sciences Research Center, State University of New York, Albany, NY 12203, USA

<sup>4</sup> College of Global Change and Earth System Science, Beijing Normal University, Beijing 100875, China

<sup>5</sup> Department of Hydrology and Atmospheric Sciences, University of Arizona, Tucson, AZ 85721-0081, USA

been summarized by some studies (Trenberth et al. 2009; Wild et al. 2013; L'Ecuyer et al. 2015). Meanwhile, modeled clouds, radiation, and precipitation agree with observations within a certain range on a global scale; however, large biases occur at the regional scale (Flato et al. 2013). Improved understanding of the interactions of clouds, radiation and precipitation and their parameterizations in climate models are one of the largest sources of uncertainty in predicting potential future climate changes (Stephens 2005; Bony et al. 2006; Boucher et al. 2013). Regional cloud-radiation-precipitation associations are therefore the subjects of increased attention.

Asian monsoon region (AMR), mainly including Eastern China (EC) and South Asia (SA), is an important region for studying clouds and precipitation. Both clouds and precipitation show strong seasonal variations over the AMR, where the summer monsoon system exhibits frequent and heavy precipitation (Webster et al. 1998; Ding and Chan 2005). The Asian monsoon not only profoundly affects regional energy and hydrological processes but also exerts an important influence on global climate changes through large-scale circulation interactions (Webster et al. 1998; Ding and Chan 2005; Wang 2006). Modeling present and projected regional climate is of importance for socio-economics over the AMR where more than 2 billion people live. Current climate models have considerable difficulty in reproducing major climatic processes over the AMR (Wang 2006; Rajeevan and Nanjundiah 2010; Boo et al. 2011) and some model biases have been attributed to clouds and radiation processes (Li et al. 2009, 2013; Stevens and Bony 2013; Wang et al. 2014; Dolinar et al. 2015). Hence, examining the scientific issues associated with CREs is crucial for understanding and predicting climate system and relevant change over the AMR.

Figure 1 presents the global annual mean total cloud fraction (CF), all-sky albedo, net CRE and radiation budget at the TOA. In addition to ice-snow covered high latitudes, most deserts in the Northern Hemisphere, the Tibetan Plateau (TP), and stratiform regions (e.g., the northern Pacific and Atlantic, southeast Pacific and Southern Ocean) also have high albedo. Note that EC is situated just to the east of the TP, and it exhibits the highest albedo ( $>0.45$ ) (Fig. 1b) and net CRE ( $-60 \text{ W m}^{-2}$ ) (Fig. 1c) of land areas at this latitude, which is a consequence of regional cloud properties (Wang et al. 2004; Yu et al. 2004). Since clouds are highly reflective, the net TOA radiation budget is negative (up to  $-20 \text{ W m}^{-2}$ ) over EC (Fig. 1d), indicating a cooling effect. In contrast, the net TOA radiation budgets around SA and the western Pacific Ocean are positive (Fig. 1d), representing a warming effect. As listed in Table 1, the climatological annual means of SW CRE (SWCRE) and net CRE over EC are evidently larger than those averaged over SA and the Northern Hemisphere. The distinguishable

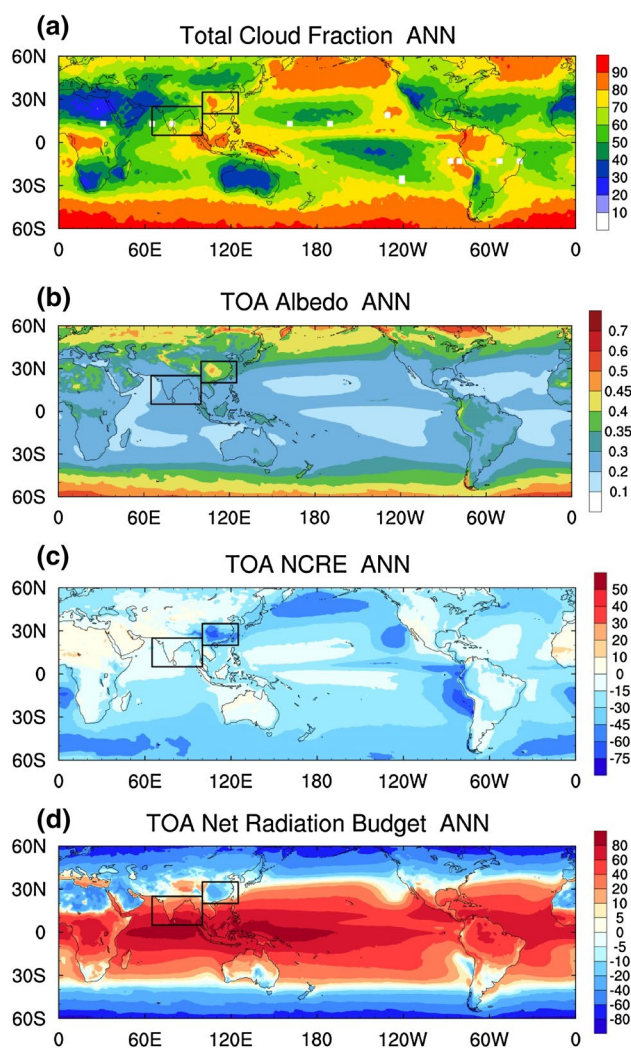


**Fig. 1** Annual mean **a** total cloud fraction (%), hereafter TCF) derived from GOCCP (GCM Oriented CALIPSO Cloud Product) during the period 2007–2014, **b** all-sky albedo, **c** net CRE ( $\text{W m}^{-2}$ , hereafter NCRE) and **d** net radiation budget ( $\text{W m}^{-2}$ ) at the TOA derived from NASA CERES-EBAF during the period 2001–2014. The *black boxes* represent the Asian Monsoon Regions (AMR) in this study, including eastern China (EC,  $20\text{--}35^\circ\text{N}$ ,  $100\text{--}125^\circ\text{E}$ ) and South Asia (SA,  $5\text{--}25^\circ\text{N}$ ,  $65\text{--}100^\circ\text{E}$ )

cloud effects over EC and SA suggest that the cloud types and properties over these two regions are different.

Although some previous studies partially revealed these different CREs over the AMR (Rajeevan and Srinivasan 2000; Wang et al. 2004; Yu et al. 2004) and noted the CRE differences between EC and SA (Yu et al. 2001; Luo et al. 2009), these studies focused primarily on a specific season and particularly lack an in-depth investigation of the annual cycle of CREs. The annual cycle is the strongest signal of the Asian monsoon climate (Webster et al. 1998; Ding 2007). Consequently, CFs and resultant CREs exhibit remarkable seasonal migration over the AMR and

**Table 1** Radiative fluxes, net budget and albedo at all-sky TOA, column total cloud fraction (TCF) and CREs averaged over EC, SA and northern hemisphere (NH)

	OLR ( $\text{W m}^{-2}$ )	RSUT ( $\text{W m}^{-2}$ )	Net budget ( $\text{W m}^{-2}$ )	Albedo	TCF (%)	TOA CRE ( $\text{W m}^{-2}$ )		
						LWCRE	SWCRE	NCRE
EC	242.24	134.79	-5.00	0.362	71.94	31.25	-73.87	-42.62
SA	251.40	99.02	50.38	0.244	60.45	36.13	-47.52	-11.39
NH	240.36	99.61	-0.12	0.318	54.21	26.44	-44.13	-17.69

are closely linked to the monsoon circulation (Chen and Liu 2005; Luo et al. 2009; Guo and Zhou 2015). Besides, CREs are sensitive to cloud types, CFs and meteorological fields (Hartmann et al. 1992; Bony et al. 1997). Many studies have indicated that LW CRE (LWCRE) is closely related to high clouds in tropical convective regions (Kiehl 1994), and SWCRE is closely related to low clouds, for example over the eastern Pacific coast where descending motion prevails (Wood and Bretherton 2006; Clement et al. 2009). Nevertheless, there has been little research on similar climatic relationships between CREs and CFs, and their seasonal variations over the AMR. On the other hand, few studies have considered how seasonal variations of CREs are linked to precipitation over the AMR. The lack of research into the factors mentioned above hinders advances in predicting cloud-radiation-precipitation processes over the AMR in climate models. Thus, it is of great importance to further characterize annual cycles of CREs and identify the similarities and differences of clouds-radiation-precipitation associations over these two regions.

The purpose of this study is to use recently satellite-based and reanalysis datasets to investigate seasonal characteristics of CREs and their associations with CFs and precipitation over the AMR from the perspective of climatological state. Since EC and SA are major sub-regions in the AMR, we focus on their annual cycles of CFs and CREs, especially on similarities and differences between summer and winter. Furthermore, we examine the relationships between CREs and column CFs as well as precipitation, and compare seasonal variations of these relationships over the two AMR sub-regions. The remainder of this paper is organized as follows. Section 2 describes the datasets and the methods used in this study. Section 3 presents the seasonal variations of CREs over the AMR. Section 4 discusses the behaviors of CREs and CFs over EC and SA, as well as their associations with precipitation in Sect. 5. Finally, conclusions and a discussion are given in Sect. 6.

## 2 Data and methods

### 2.1 Observational and reanalysis datasets

The TOA radiative fluxes in this study are obtained from NASA Clouds and the Earth's Radiant Energy System

(CERES), utilizing the most recent CERES Energy Balanced and Filled at the TOA (EBAF-TOA) Ed2.8 dataset (Doelling et al. 2013). The CERES-EBAF includes incident SW flux and outgoing SW and LW radiative fluxes at the TOA under clear-sky and all-sky conditions. This dataset has been widely used in studying the role of clouds and the energy cycle in the earth-climate system (Loeb et al. 2009; Wild et al. 2013). Thus, it is considered as the observational radiation dataset herein. The CERES dataset has a high spatial resolution of  $1.0^\circ$  latitude by  $1.0^\circ$  longitude and is available from March 2000 to December 2014.

Cloud properties, including CFs, cloud (liquid and ice) water path and particle sizes, are taken from CERES-Moderate-resolution Imaging Spectroradiometer (hereafter, MODIS) SYN1 edition 3 datasets (Minnis et al. 2011a, b), with the same data length and horizontal resolution as CERES-EBAF. Meanwhile, total, high-, middle-, and low- cloud fraction (hereafter TCF, MCF, LCF and LCF) and 3-dimensional (3D) cloud vertical distributions are from the general circulation model (GCM) Oriented CALIPSO Cloud Product (GOCCP). GOCCP data are based on CALIPSO satellite datasets, designed to evaluate the cloudiness simulated in climate models (Chepfer et al. 2010) and have shown their value in climate analysis (Cesana and Chepfer 2012; Boucher et al. 2013). GOCCP data have a horizontal resolution of  $2.0^\circ$  latitude by  $2.0^\circ$  longitude, with 40 levels in the vertical at 480 m intervals, and cover the period from June 2006 to December 2014. In addition to CERES-MODIS cloud properties, we also use cloud water path (CWP) derived from CloudSat Radar-Only Cloud Water Content Product (2B-CWC-RO) (version R04) satellite products (Austin et al. 2009). These data also include cloud liquid and ice water path (LWP and IWP, respectively) from total and no-precipitating (no-Pcp) particles. The total- and no-Pcp CWP (LWP and IWP) are identical to those used in studies by Jiang et al. (2012) and Wang et al. (2014). The data cover the period from June 2006 to December 2010 and have a spatial resolution of  $2.0^\circ$  latitude by  $2.0^\circ$  longitude.

The total precipitation (hereafter, precipitation) dataset is taken from Global Precipitation Climatology Project (GPCP) monthly products with  $2.5^\circ$  latitude by  $2.5^\circ$  longitude global resolution from 1979 to the present (Adler et al. 2003), which shows good abilities in representing the climatological state of precipitation (Yin et al. 2004; Huffman

et al. 2009). Meteorological data come from ERA-Interim reanalysis (Dee et al. 2011), including horizontal wind, vertical velocity and humidity, and have the spatial resolution of  $1.0^\circ$  latitude by  $1.0^\circ$  longitude. The period of ERA-Interim is the same with GPCP and have considerable performance in well reproducing meteorological state (Simmons et al. 2010, 2014). The cloud properties as well as their estimated uncertainties are summarized in Table 2. Since GOCCP data are derived from active CALIPSO, their high and low CFs, as expected, are higher than those derived from passive remote sensors, such as MODIS and International Satellite Cloud Climatology Project (ISCCP) (Stubenrauch et al. 2013). Compared with CWP, CF data have smaller uncertainties. This study therefore focuses on CFs from GOCCP for the analysis of quantitative relationships.

## 2.2 Analysis methods

Following previous work (Ramanathan et al. 1989; Boucher et al. 2013), TOA CREs in this study are defined as the differences in TOA radiative fluxes between clear-sky and all-sky conditions:

$$LWCRE = OLRCS - OLR, \quad (1)$$

$$SWCRE = RSUTCS - RSUT, \quad (2)$$

$$NCRE = LWCRE + SWCRE, \quad (3)$$

where OLRCS and OLR are outgoing longwave (LW) radiative fluxes at the TOA under clear-sky and all-sky conditions, respectively; RSUTCS and RSUT are the corresponding outgoing SW radiative fluxes; and net CRE (NCRE) is the arithmetic sum of LWCRE and SWCRE. The radiative fluxes and CREs in this study are for the TOA without special description.

In this study, the climatology of TOA radiative fluxes and CREs, CERES-MODIS cloud properties and

meteorological fields is derived from the period 2001–2014. The relationship between CREs and CFs from GOCCP are calculated from the period 2007–2014 due to limited dataset from GOCCP. To have reasonable comparisons from different datasets with different spatial resolutions, the variables with higher resolution are re-gridded into lower resolution using bilinear interpolation, e.g.,  $1.0^\circ \times 1.0^\circ$  of CERES-EBAF into  $2.0^\circ \times 2.0^\circ$  of GOCCP. The domains of EC and SA are selected as  $20\text{--}35^\circ\text{N}$ ,  $100\text{--}125^\circ\text{E}$  and  $5\text{--}25^\circ\text{N}$ ,  $65\text{--}100^\circ\text{E}$ , respectively, following the definitions of these regions in previous studies (Yu et al. 2001; Wang et al. 2004; Li et al. 2009). As a large number of abbreviations are used in this study, for convenience a list of the abbreviations is presented in Table 3.

## 3 Seasonal variations of CREs over the AMR

### 3.1 The contrast between summer and winter CREs

Figure 2 illustrates TOA CREs over the AMR in winter (December–January–February) and summer (June–July–August) and demonstrates remarkable seasonal contrasts of CREs over the AMR. In winter, both LWCRE and SWCRE are weak over SA (Fig. 2a, c). SWCRE is stronger over EC than over SA (Fig. 2c). The spatial distributions of LWCRE and SWCRE in Fig. 2 are strongly associated with TCF and all-sky TOA albedo. For example, SWCRE over the Sichuan Basin during winter are very high, and correspond to the high TCF and TOA albedo (Fig. 3c, e). In summer, as shown in Fig. 2b, d, both LWCRE and SWCRE evidently increase over the entire AMR, with large CREs occurring in the western Indian Peninsula, northeastern Bay of Bengal (BOB), and from the eastern South China Sea to the Philippine Sea where active convection prevails (Fig. 3j). The spatial distribution of LWCRE is similar to that of precipitation (Fig. 3b) and vertical motion at 500 hPa (Fig. 3j) where

**Table 2** Global monthly mean cloud products used in this study

Data source	Grid spacing and period	Products	Estimated uncertainty
CERES-MODIS	$1.0^\circ \times 1.0^\circ$ 03/2000–12/2014	CF	7% <sup>a</sup>
		CWP	Factor of 2 <sup>b</sup>
CALIPSO-GOCCP	$2.0^\circ \times 2.0^\circ$ 07/2006–12/2014	CF	4–5% <sup>c,d</sup>
CloudSat	$2.0^\circ \times 2.0^\circ$ 07/2006–12/2010	CWP	Factor of 2 <sup>b</sup>

<sup>a</sup>Minnis et al. (2011b)

<sup>b</sup>Jiang et al. (2012)

<sup>c</sup>Mace et al. (2009)

<sup>d</sup>Stubenrauch et al. (2013)

**Table 3** Abbreviation and variable names used in this study

Abbreviation	Full name
AMR	Asian monsoon region
AOD	Aerosol optical depth
BOB	Bay of Bengal
CC	Correlation coefficient
CF	Cloud fraction
CRE	Cloud radiative effect
CERES	Clouds and the Earth's Radiant Energy System
EC	Eastern China
EBAF	Energy balanced and filled
GOCCP	GCM Oriented CALIPSO Cloud Product
HCF	HCF high-level cloud fraction
ISCCP	International Satellite Cloud Climatology Project
LCF	Low-level cloud fraction
LWCRE	LWCRE longwave cloud radiative effect
LWP	Liquid cloud water path
MCF	Middle-level cloud fraction
MODIS	MODIS the Moderate-resolution Imaging Spectro-radiometer
NCRE	Net cloud radiative effect
NSWCRE	Normalized shortwave cloud radiative effect
OLR	Outgoing longwave radiation
Re	Effective radius
RH	Relative Humidity
SA	South Asia
SWCRE	SWCRE shortwave cloud radiative effect
TCF	Total cloud fraction
TP	Tibetan Plateau
TOA	Top of the atmosphere

the strong precipitation corresponds well with strong ascending motion, and results in large positive LWCRE. Large SWCRE over EC (Fig. 2d) is strongly associated with high TCF (Fig. 3d) and all-sky TOA albedo (Fig. 3f).

Although a seasonal contrast over the AMR is clear, there are some differences in CREs between EC and SA. As shown in Fig. 2g, h, the SWCRE in winter ( $-56.8 \text{ W m}^{-2}$ ) is less than that in summer ( $-88.3 \text{ W m}^{-2}$ ), with the ratio between them being 0.64 over EC, much higher than the corresponding ratio (0.23) over SA. The corresponding ratio of LWCRE has values over EC and SA of 0.39 and 0.28, respectively, closer than the values for SWCRE. Due to the presence of relatively larger SWCRE over EC in winter (Fig. 2g), NCRE over EC ( $-38.5 \text{ W m}^{-2}$ ) is much larger than that over SA ( $-3.1 \text{ W m}^{-2}$ ) (Fig. 2g, h). The difference shown here indicates that the seasonal characteristics of CRE over the AMR differ over EC and SA, particularly for SWCRE.

### 3.2 Annual cycles of CREs over EC and SA

To further quantitatively examine seasonal variations, Fig. 4 provides annual cycles of TOA CREs, all-sky albedo and CRE-related ratios averaged over EC and SA. Over SA, the CREs (LWCRE, SWCRE and NCRE) are the weakest in February and then gradually increase until reaching a peak in July (Fig. 4a), varying in-phase. Over EC, the monthly means of LWCRE and SWCRE have the weakest (strongest) value in January (June) (Fig. 4b). The ratio of the magnitudes of  $-LWCRE$  to SWCRE is used to measure the contribution of SWCRE to the NCRE. Figure 4c clearly shows that the ratios over SA increase from summer months to winter months with an annual average of  $\sim 0.8$ , indicating that LW warming and SW cooling effects compensate each other and result in relatively weaker NCRE. Contradicting to the ratios over SA, the ratios ( $-LWCRE/SWCRE$ ) over EC are much lower but peak during summer months and decline in cold months (Fig. 4d). Therefore, SW cooling effect is dominant over EC, especially in winter and spring, which leads to a remarkable TOA cooling effect on regional atmospheric-surface climate system. In addition, due to the different seasonal amplitudes of SWCRE and LWCRE over EC, the largest NCRE ( $-56.1 \text{ W m}^{-2}$ ) appears in May.

As shown in Fig. 4d, TOA albedo over EC is the strongest in January and its annual cycle is also opposite to that over SA (Fig. 4c). Albedo and SWCRE are determined by both incident sunlight and local cloud properties. To emphasize local cloud effects, the normalized SWCRE (NSWCRE) is used here:

$$NSWCRE = -SWCRE/RSDT, \quad (4)$$

where RSDT is TOA incident SW radiation flux. After TOA incident solar radiation is excluded, both NSWCRE and albedo over EC are larger in winter (Fig. 4d), when cloud physical properties are major factors influencing SWCRE except for incident solar radiation. Albedo and NSWCRE over SA are still in phase with regional CREs (Fig. 4c).

### 3.3 Differences in SWCRE during cold months

Given the large differences of SWCRE over EC and SA in cold months, people could not help to ask what cause these differences? One possible reason is the different synoptic patterns over these two regions. In winter, moderate ascending motion at 500 hPa occurs over EC while most of the SA areas are controlled by large-scale subsidence motion (Fig. 3i). Winter ascending motion over EC is connected with the TP and surrounding land-ocean topography, and the westerly jet over the middle Northern Hemisphere reaches a maximum in winter (Wu et al. 2007).

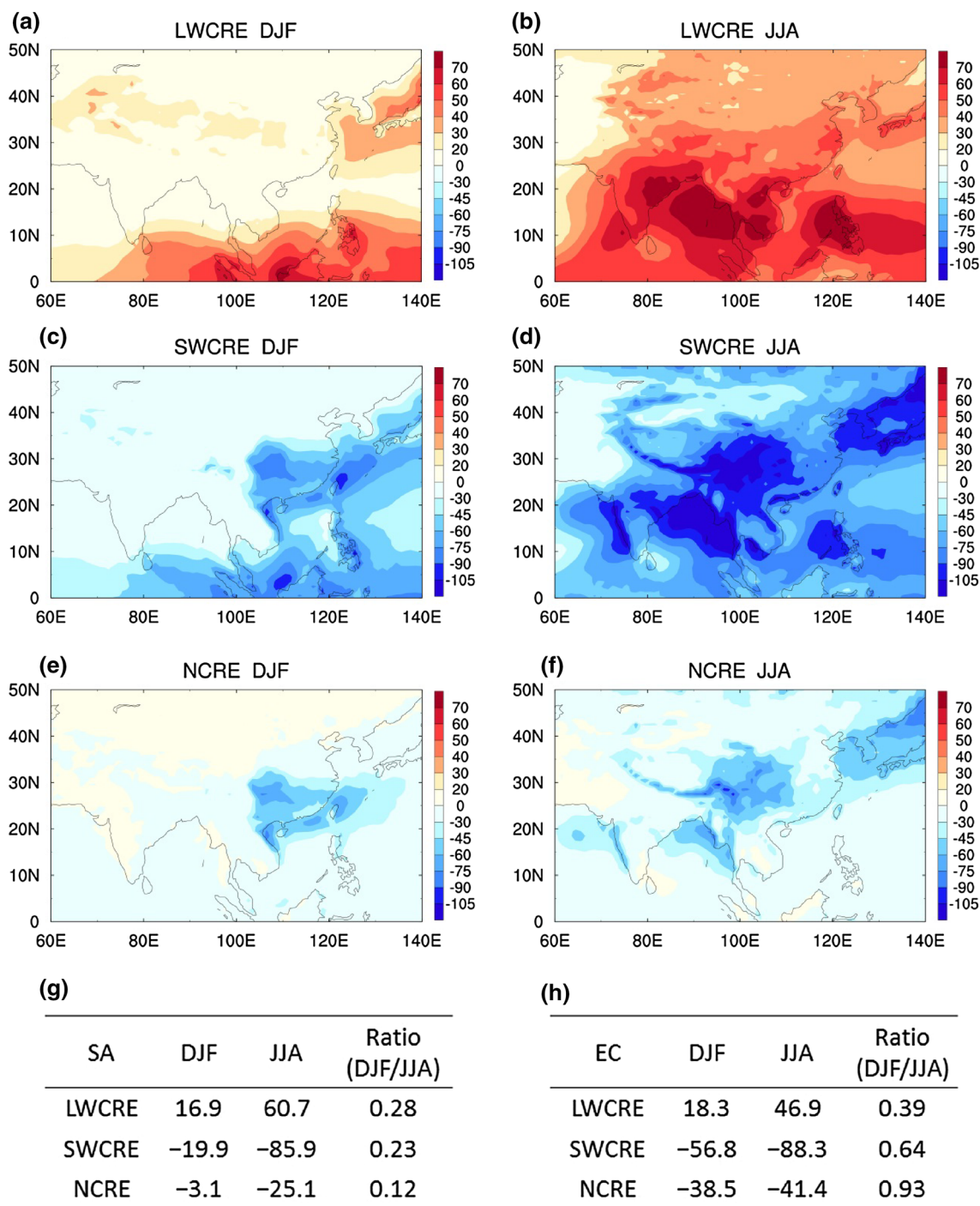


**Fig. 2** Climatological mean distributions of **a** LWCRE, **c** SWCRE and **e** NCRE over the AMR during the winter months (December–January–February: DJF) for the period 2001–2014; **b**, **d** and **f** are the same as (**a**, **c**, **e**) but for the summer months (June–July–August: JJA).

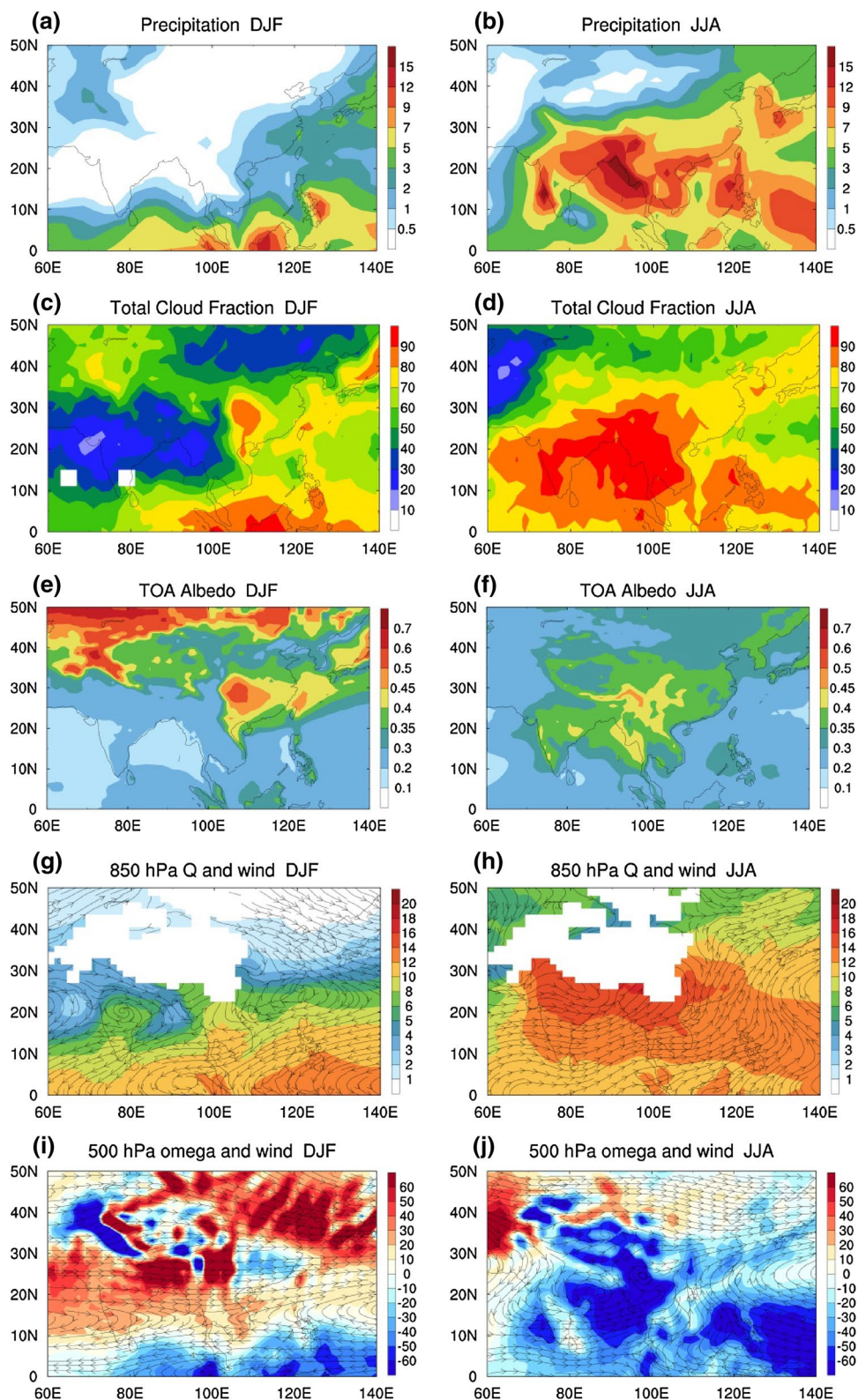
**g** CREs averaged over SA in DJF and JJA and the ratios between the two seasons. **h** Is the same as (**g**) but for EC. Units are  $W m^{-2}$  except for the ratios in (**g**, **h**)

These dynamical conditions produce low-level southwesterly circulation and middle-level divergence east to the TP (Fig. 3g, i). Furthermore, water vapor transported from the southwest and south into EC provides a source of cloud water (Fig. 3g). These circulation conditions favor the

formation of persistent stratus clouds, which tend to produce large SWCRE over EC during winter (Yu et al. 2004; Li and Gu 2006).

Another possible reason arises from cloud properties related to the circulation. Figure 5 displays cloud LWP,

**Fig. 3** Climatological mean distributions over the AMR for the period 2001–2014 in winter (*left panels*) and summer (*right panels*). **a** Total precipitation ( $\text{mm d}^{-1}$ ) (hereafter, precipitation), **c** TCF (%), **e** all-sky TOA albedo, **g** horizontal wind streamlines and specific humidity ( $10^3 \text{ kg kg}^{-1}$ ) at 850 hPa and **i** horizontal wind streamline and vertical velocity ( $\text{hPa d}^{-1}$ ) at 500 hPa; **b**, **d**, **f**, **h** and **j** are as (**a**, **c**, **e**, **g**, **i**), respectively



cloud particle sizes and aerosol optical depth (AOD). SWCRE is strongly affected by low-level cloud properties (Hartmann et al. 1992), so only liquid cloud properties are listed here. In winter, LWPs retrieved by MODIS over EC

are much larger than those over SA, while the LWP values from CloudSat over EC and SA show a smaller difference between EC and SA. Note that LWPs from both satellites are larger over EC than over SA in spring (Fig. 5a, b). The

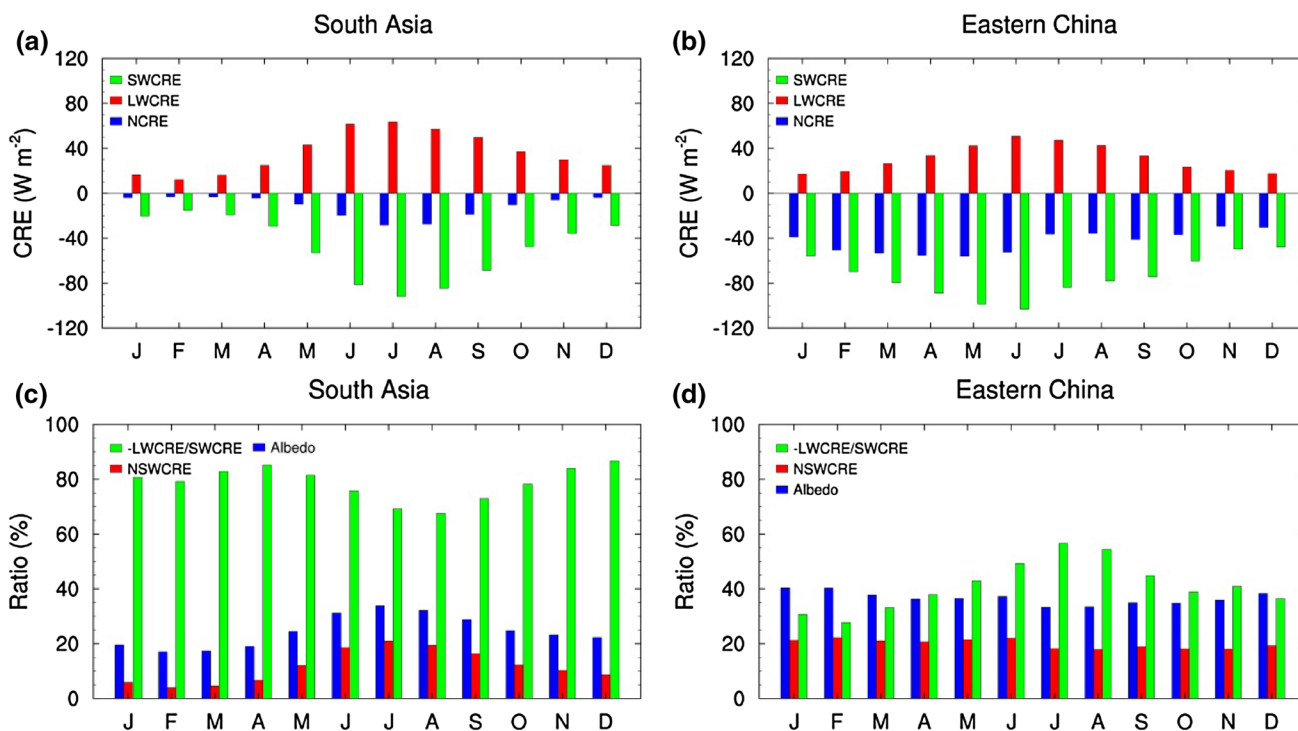


**Fig. 4** Annual cycles of **a, b** SWCRE, LWCRE, and NCRE ( $W m^{-2}$ ), and **c, d** all-sky albedo, the ratio (%) of LWCRE to SWCRE, and NSWCRE (SWCRE divided by incident solar radiative

flux, hereafter NSWCRE) during 2001–2014. **a** and **c** Are averaged over SA; **b** and **d** are averaged over EC

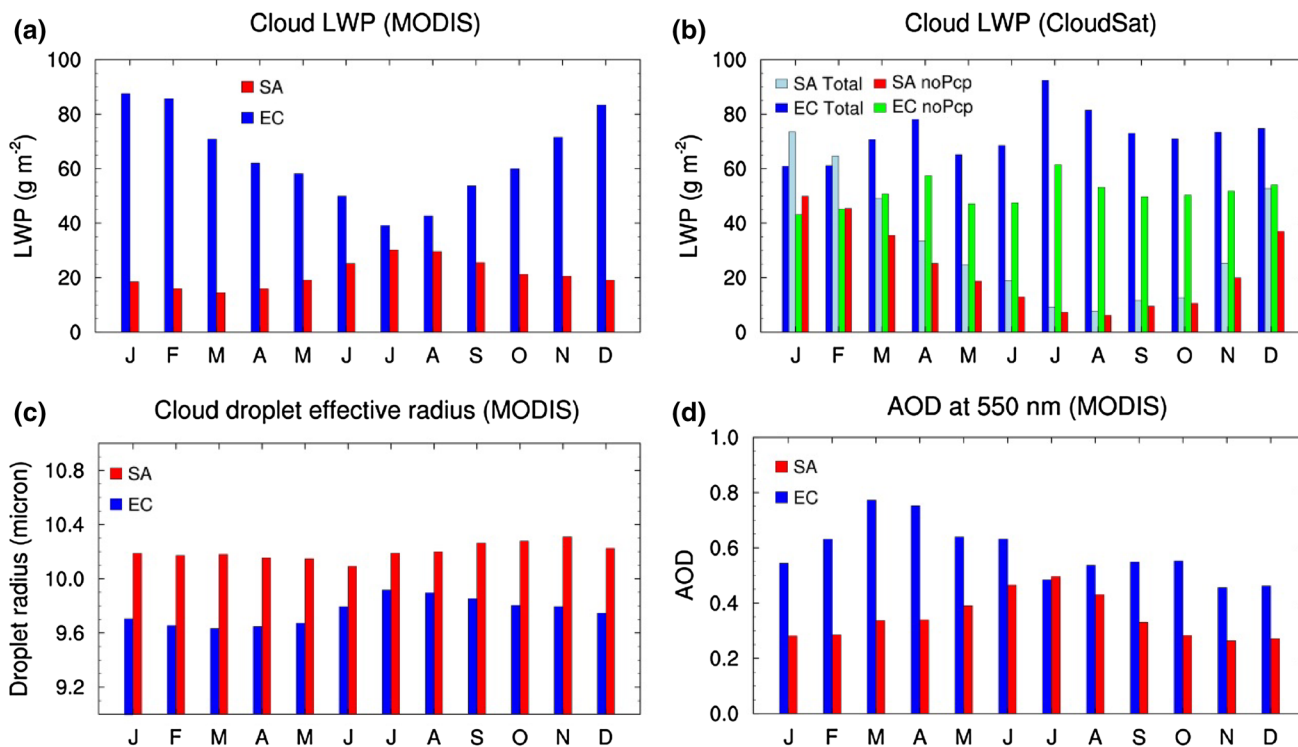


**Fig. 5** Annual cycles of **a** cloud liquid water path (LWP) from MODIS, **b** cloud LWP from CloudSat, **c** droplet radius at the cloud top from MODIS, and **d** aerosol optical depth (AOD) at 550 nm aver-

aged over EC and SA during 2001–2014. Note that the LWPs derived from CloudSat are averaged from 2007 to 2010

regional mean AOD over EC is much higher than over SA, especially in winter (Fig. 5d), suggesting that aerosol concentration is higher over EC.

During winter and spring, convection is weak over EC and SA. In this situation, given constant cloud water, higher AOD tends to produce more cloud droplets and reduces their particle size (Albrecht 1989). In fact, Fig. 5c also shows that winter effective radius ( $R_e$ ) at the top of liquid cloud over EC is larger than over SA. Thus, according to the following diagnose relationship by Cess et al. (1990),

$$\tau \sim \frac{3LWP}{2R_e}, \quad (5)$$

where  $\tau$  and  $R_e$  are liquid cloud optical depth and effective radius, respectively. When LWP is larger over EC during winter and spring, smaller  $R_e$  causes larger  $\tau$ . Smaller  $R_e$  caused by higher AOD over EC consequently produces larger  $\tau$  with stronger cloud optical scattering and extinction. Besides, lower air temperature in winter acts against the conversion from cloud water to precipitation but favor the suspension of more cloud water in the air and a prolongation of cloud albedo effects (Twomey 1977). Thus, the TOA cloud albedo effect (SWCRE) is intensified over EC in winter and spring. Previous work by Yu et al. (2004), Li and Gu (2006), and Zhang et al. (2013) proved that abundant stratus clouds over EC associated with the TP dynamical forcing directly contribute to strong regional SWCRE in winter. Apart from these circulation effects, our analysis indicates that cloud micro-characteristics (small cloud liquid particle, high cloud liquid content and albedo) also favor persistent SWCRE over EC during winter and spring. Ground-based observations by Liu et al. (2013) also showed that the strongest cloud optical depth and smallest  $R_e$  over EC appear in winter, partially supporting our analysis. In summer, LWP over EC, particularly no-Pep LWP, is apparently larger and  $R_e$  is still smaller relative to SA (Fig. 5a–c), which favors larger SWCRE for EC. With the coming of the summer monsoon, cloud layers increase and have a more complicated vertical distribution over the AMR. The effects of CFs on CREs in summer are discussed further in the next section.

#### 4 Association of CREs with column CFs

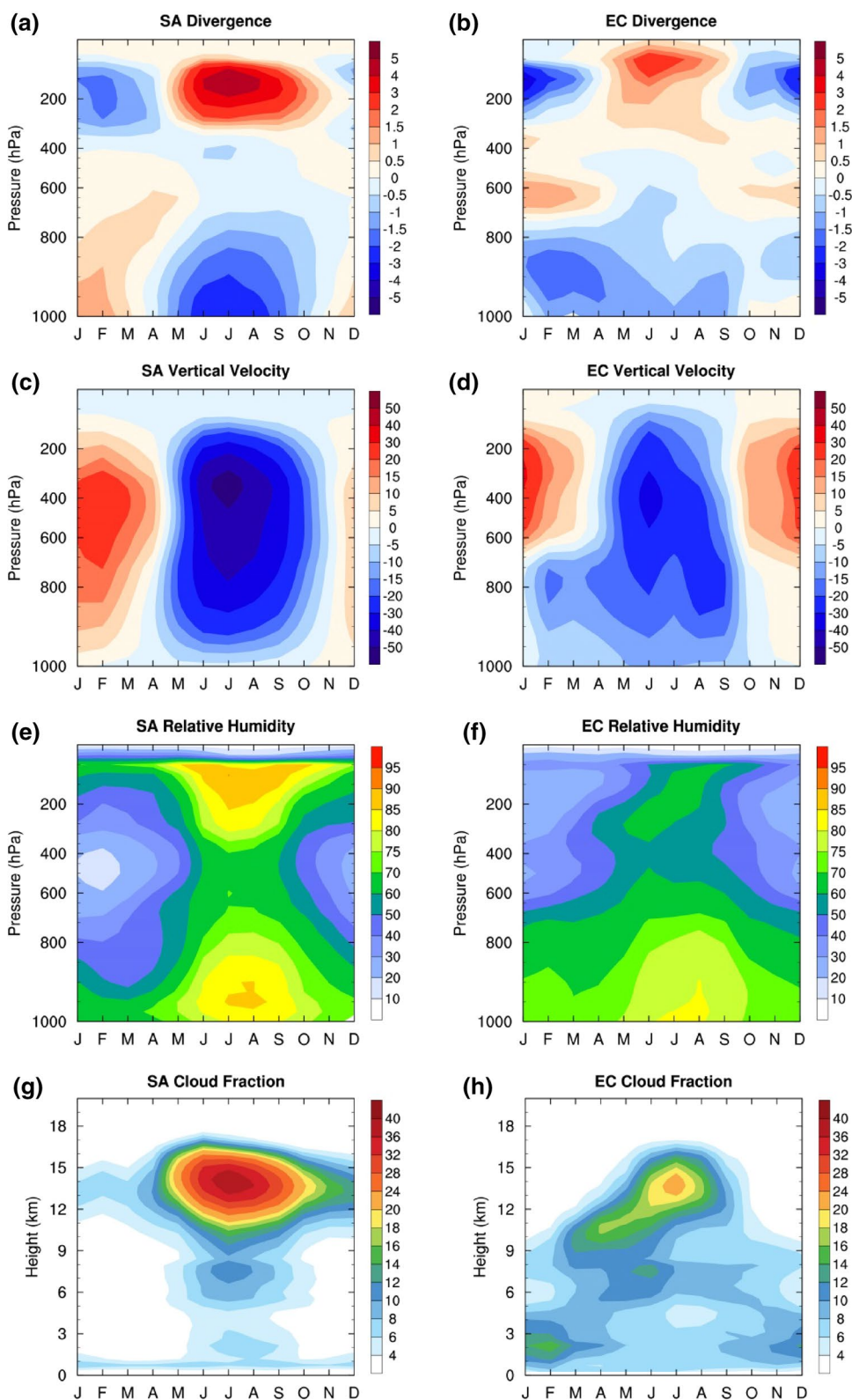
Given that CREs depend strongly on column CFs, we examine here the sensitivities of CREs to CFs over the AMR with an emphasis on column TCF, HCF and LCF. The GOCCP record is too short with only 8 years of column and vertical CFs, so the analysis in this section focuses on their climatological state. Figure 6 presents seasonal changes in the vertical distributions of divergence, vertical velocity, relative humidity (RH), and CFs over the two regions. Over

SA, evident low-level divergence and high-level convergence appear in winter, but tropospheric convergence and vertical motion are opposite to that in summer when strong ascending motion and high RH prevail (Fig. 6a, c, e). CFs over SA mostly consist of HCF (Fig. 6g). Over EC, strong low-level convergence and middle-level divergence occur from winter onwards, corresponding to moderate ascending motion and RH, and develop into deeper ascending motion in summer (Fig. 6b, d, f). These favorable dynamical conditions over EC lead to lots of LCF starting from the winter (Fig. 6h). With the advance of the summer monsoon, deep convection enhances HCF and MCF over EC and SA. Unlike to SA, LCF change little with season over EC (shown in Fig. 9f), which was also pointed out by Luo et al. (2009).

These differences in CFs between EC and SA are consequently reflected in their CREs. Figures 7 and 8 show the relationships between CREs and column CFs. Over SA, the correlation coefficient (CC) between LWCRE and TCF (HCF) is 0.96 (0.98) in winter (Fig. 7a, b) and with corresponding values of 0.63 (0.87) in summer (Fig. 8a, b). The CCs between SWCRE and TCF over SA reach  $-0.96$  and  $-0.80$ , respectively, in winter and summer (Figs. 7e, 8e). It is noteworthy that the CC between SWCRE and HCF is also very high, with the values of  $-0.95$  and  $-0.65$  in winter and summer, respectively (Figs. 7i, 8i). Over EC, the CC between LWCRE and TCF (HCF) is quite low in winter (Fig. 7c, d); with the increase in HCF, the CC between LWCRE and HCF can increase to 0.63 in summer (Fig. 8d). Due to small LCF, the CC between SWCRE and LCF is not high over SA (Figs. 7f, 8f). In contrast, because LCF accounts for a larger proportion of CFs over EC, the CC between SWCRE and LCF is  $-0.81$  over EC in winter (Fig. 7h). With the increases in HCF in summer, the CC between SWCRE and HCF increase to  $-0.51$  over EA (Fig. 8j).

In addition to winter and summer, we further analyze annual cycles of CCs between CREs and column CFs. The CCs between LWCRE and TCF (HCF) over SA are high ( $>0.9$ ) in most months (Fig. 9a); The CCs decrease somewhat in summer with the increase in CF and complex of its vertical distribution, but are still  $>0.8$  because of the dominance of HCF (Fig. 9e). Note that the CCs between SWCRE and HCF are even comparable to CCs between LWCRE and HCF over SA during the whole year (Fig. 9c). South Asia is in a tropical area where deep convection readily produces HCF with large amounts of cloud water. The optical depth caused by this kind of HCF makes up a large fraction of total cloud optical depth (Rossow and Schiffer 1999; Rajeevan and Srinivasan 2000). These features very likely lead to good relationships between SWCRE and HCF over SA. Over EC, the CCs between SWCRE and LCF

**Fig. 6** Annual cycles of vertical profiles of **a** horizontal divergence ( $10^6 \text{ s}^{-1}$ ), **c** vertical velocity ( $\text{hPa d}^{-1}$ ), **e** relative humidity (%) and **g** CF (%) averaged over SA. **b, d, f, h** are for EC. The data period is 2001–2014, but CF from GOCCP is for 2007–2014



are high ( $>0.6$ ) during cold months (November–March) (Fig. 9d), but CCs decrease during warm months (May–October) when the proportion of LCF lowers. The CCs between LWCRE and HCF are relatively high ( $>0.6$ )

during February–April and July–August (Fig. 9b) and CCs between SWCRE and HCF (TCF) are also high during June–September (Fig. 9d). The results presented here indicate that CCs between CREs and the no-predominant

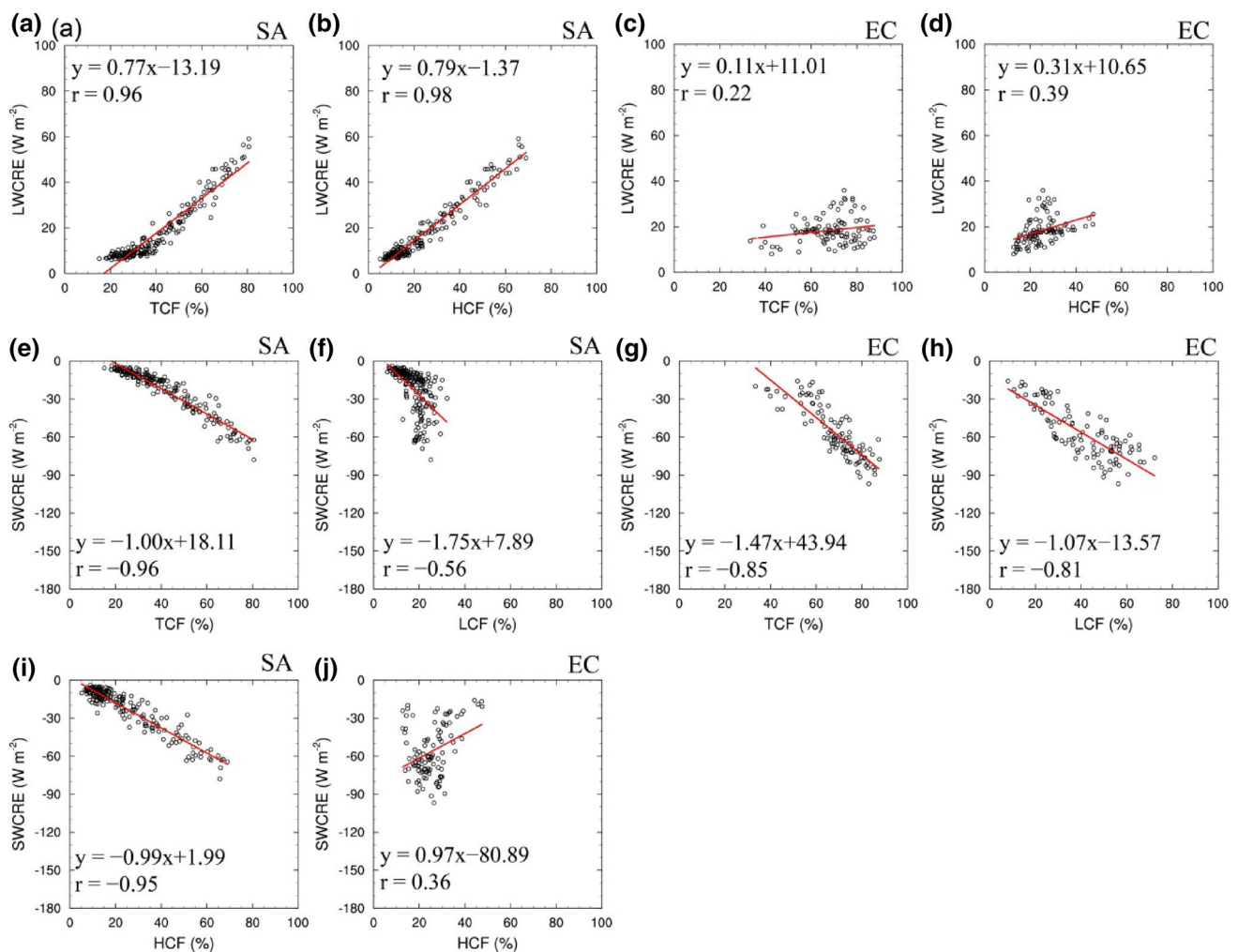


**Fig. 7** Scatter plots of climatological mean CREs and column CFs over the AMR: LWCRE versus **a** TCF and **b** high CF (HCF) over SA (5–25°N, 65–100°E), respectively; SWCRE versus **e** TCF and **f** low CF (LCF) over SA, respectively. **c–d, g–h** Are for correspond-

ing plots over EC (20–35°N, 100–125°E); SWCRE versus HCF over **i** SA and **j** EC, respectively. The period is winter of 2007–2014. Linear correlation coefficients and regression lines (*red*) are shown in each sub-plot

CF are quite low, such as the CCs between SWCRE (LWCRE) and LCF (HCF) over SA (EC) in most months. During cold months when cloud vertical structure are relatively simple over the AMR, relationships between CREs and the dominant clouds are very close, but the corresponding relationships weaken in summer when cloud structure becomes complicated (Wang et al. 2004; Rajeevan et al. 2013). Moreover, the above results show that HCF strongly affect both LWCRE and SWCRE over SA, and similar close relationship between SWCRE (LWCRE) and HCF also occurs in EC during summer. As mentioned above, existing studies focus on SA for the relationship between CREs and cloud characteristics. Since regional climatic features including general circulation, clouds types and vertical distribution have significantly differences over SA and EC, more studies of the

relationships between CREs and cloud characteristics over EC, especially vertical structure aspects, are needed in the future.

### 5 Association of CREs with precipitation

Apart from the effects of CFs, CREs are also determined by other cloud macro- and micro-physical properties, such as cloud height, cloud water content, cloud radius and their vertical distributions (Kiehl 1994; Hartman et al. 2001). The formation of these cloud micro- and macro-properties and their spatial distributions are influenced by general circulation at different spatial scales (Bony 1997). It is also known that precipitation processes are closely related to general circulation and cloud micro-processes (Rogers

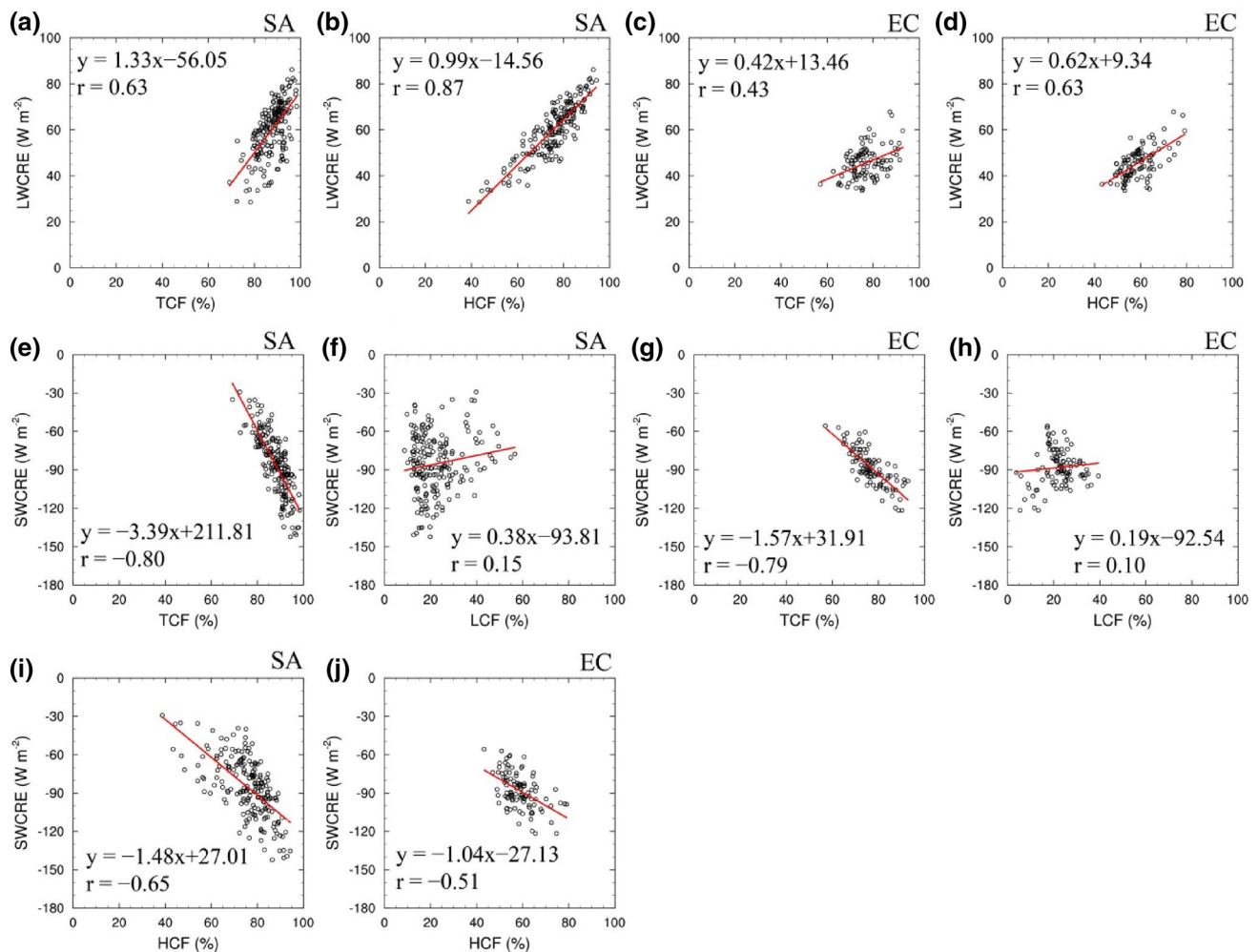


**Fig. 8** The same as Fig. 7 but for summer

and Yau 1989). Thus, to some extent, CREs are implicitly related to precipitation through general circulation and cloud properties determining CREs. Considering the great roles of clouds and precipitation as mentioned above, the comparison of quantitative correlation between CREs and precipitation over EC and SA is therefore important to explore their underlying physical relationships. Figure 10 shows latitude-time plots of monthly total precipitation, TCF and CREs over EC and SA. A clear single-peak feature is present for precipitation over SA (Fig. 10a). The peak occurs in July and the minimum in February. The seasonal cycles of TCF and CREs (LWCRE and SWCRE) are consistent with that of precipitation over SA (Fig. 10c, e, g). Their maximum zones are located around 20°N. This consistency further reveals that TCF and CREs over SA are strongly affected by monsoon processes and that they are in phase. Over EC, significant precipitation appears over 25–30°N from February and reaches a maximum by June (Fig. 10b). As the monsoon progresses, strong precipitation

moves north of 40°N over EC. The latitudinal evolution of TCF is basically similar to that of precipitation, but its central position and duration are different. For instance, large TCF over EC starts from January (Fig. 10d). LWCRE over EC evolves like precipitation and both have similar seasonal variations (Fig. 10f). As shown in Fig. 10b, h, the magnitude of precipitation over EC is not large during winter and early spring while SWCRE is strong. The annual cycle of SWCRE is different to those of precipitation and LWCRE.

We further examine the temporal correlation between precipitation and CREs by considering the similarity of their annual cycles. The climatological monthly precipitation and CREs are first obtained for the period 2001–2014 first and then the local correlations of their annual cycles are calculated at each grid point. Figure 11 displays the distribution of these local correlations over the AMR. The correlation between LWCRE and precipitation is very high and exceeds 0.9 over SA, EC and western Pacific regions, with

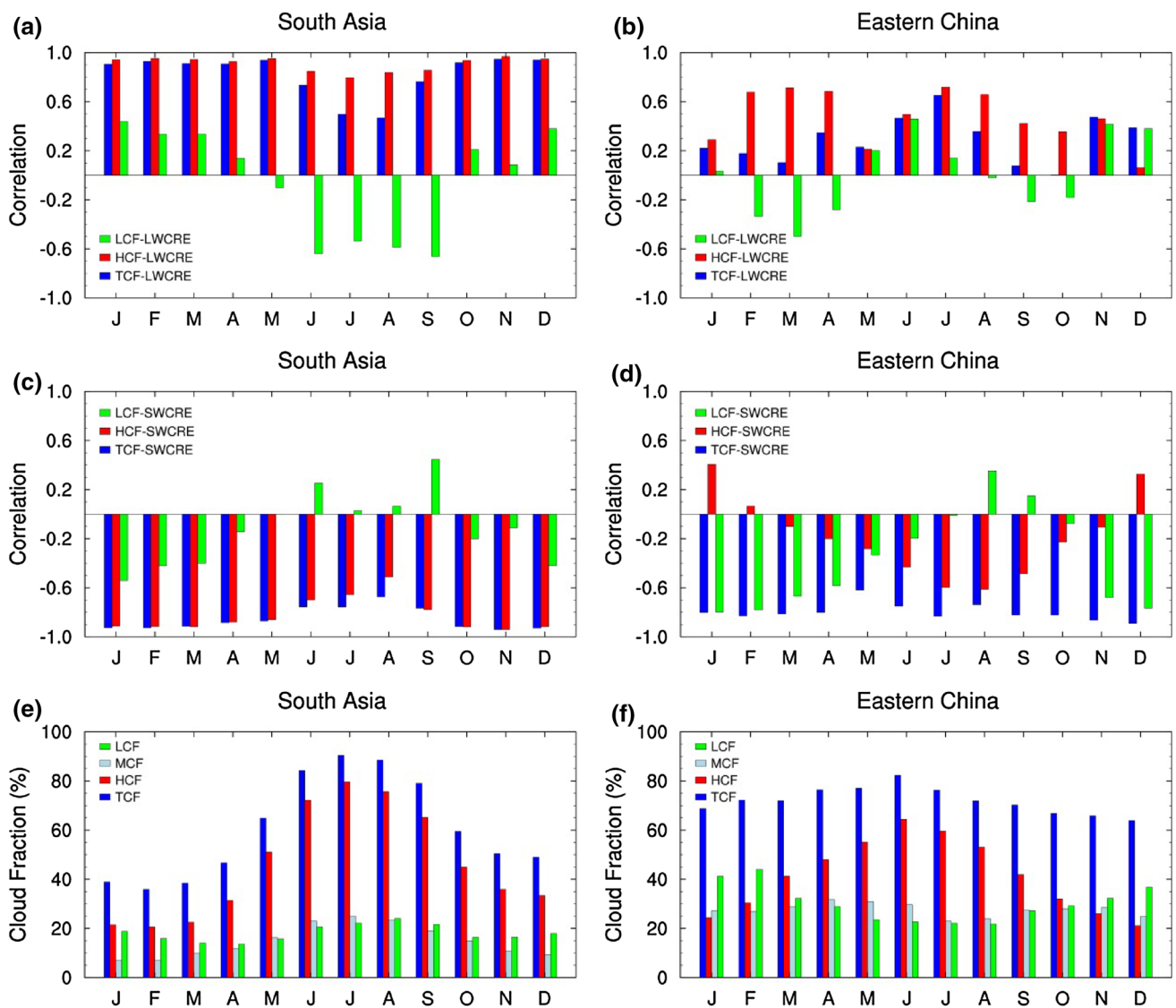


**Fig. 9** Annual cycles of correlation coefficients between **a** LWCRE and **c** SWCRE and CFs (TCF, HCF, MCF and LCF) averaged over SA, respectively. **b, d** Are the corresponding annual cycles averaged

over EC. **e, f** Are annual cycles of low, middle, high, and total CFs (%) over SA and EC, respectively. The data period is 2007–2014

the maximum ( $>0.99$ ) occurring over the BOB (Fig. 11a). This means that the annual cycles of LWCRE and precipitation are very close and in phase over the AMR. The correlation between SWCRE and precipitation is also quite high ( $>-0.95$ ) over SA and the largest value occurs in the BOB. The correlation between SWCRE and precipitation obviously decreases over EC and the regional mean is less than  $-0.70$  (Fig. 11c). In northern South China and the ocean adjacent to EC, the correlation between SWCRE and precipitation is even positive (Fig. 11b). This relatively lower temporal correlation between SWCRE and precipitation is mainly caused by their inconsistent seasonal variation over EC.

Because strong precipitation occurs frequently in summer, we analyze its summer spatial correlation with CREs over the AMR. Figure 12 shows time series of summer mean spatial correlations between CREs and precipitation over EC and SA for the period 2001–2014. The spatial correlation between LWCRE and precipitation is high over EC and SA, with mean values of over 0.63 and 0.73, respectively (Fig. 12a), indicating a good spatial correspondence. The average value over EC is higher than that over SA, which is due to the domain selection. The correlation between SWCRE and precipitation is still high over SA, with a mean value is up to  $>-0.83$ , but is very low over EC (Fig. 12b).

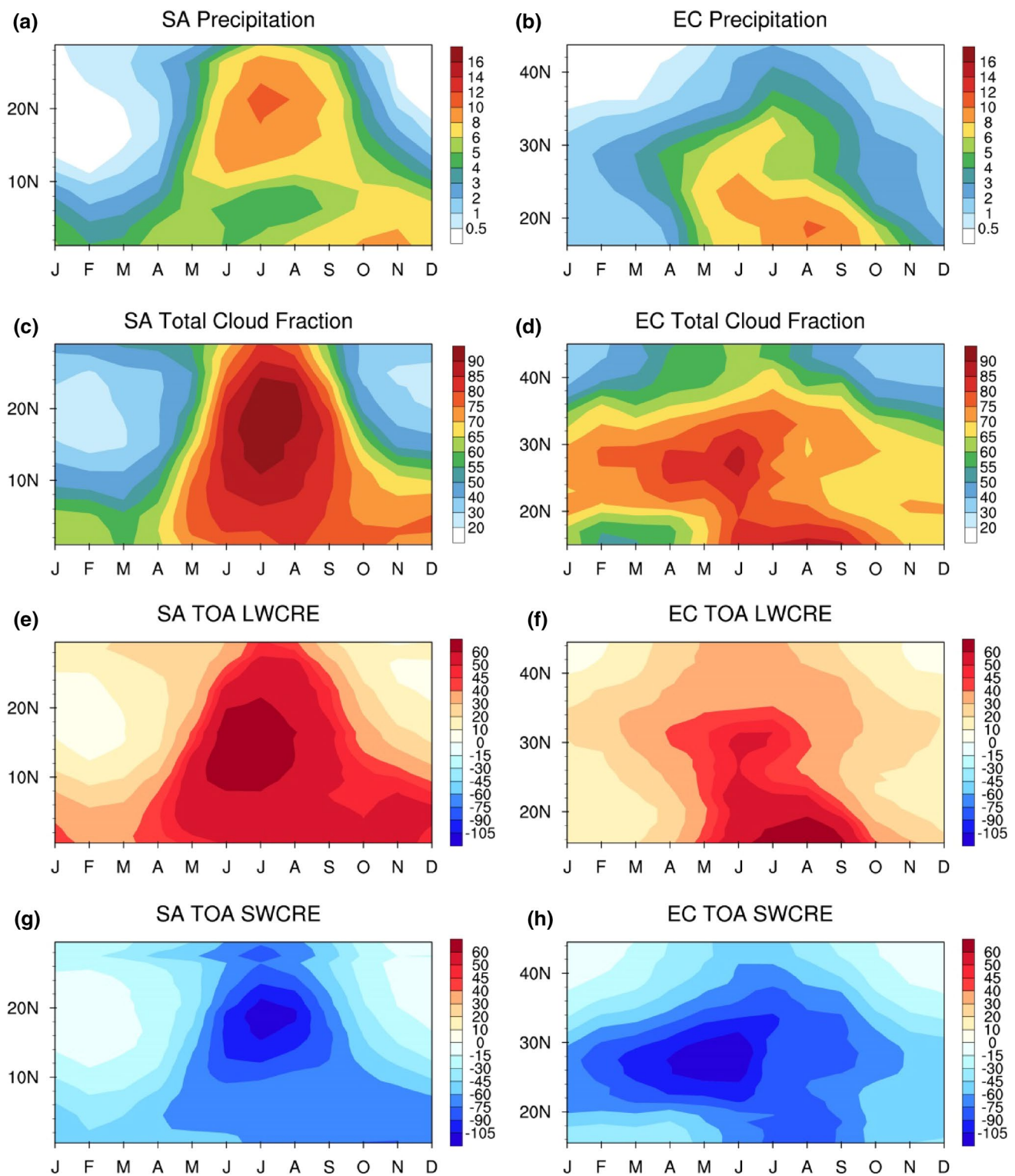


**Fig. 10** Annual cycles of **a** precipitation ( $\text{mm d}^{-1}$ ), **c** TCF (%), **e** LWCRE, and **g** SWCRE over SA ( $65\text{--}100^\circ\text{E}$ ). **b**, **d**, **f**, **h** Are the corresponding plots for EC ( $100\text{--}125^\circ\text{E}$ ). TCF is based on the period 2007–2014. Other variables are based on the period 2001–2014

Based on above results, it is clear that the annual cycles of LWCRE and SWCRE over SA are consistent with that of precipitation and then strongly modulated by

monsoon circulation. In addition, the correlation between LWCRE and precipitation over EC is also high, particularly in summer. The LWCRE are strongly related to

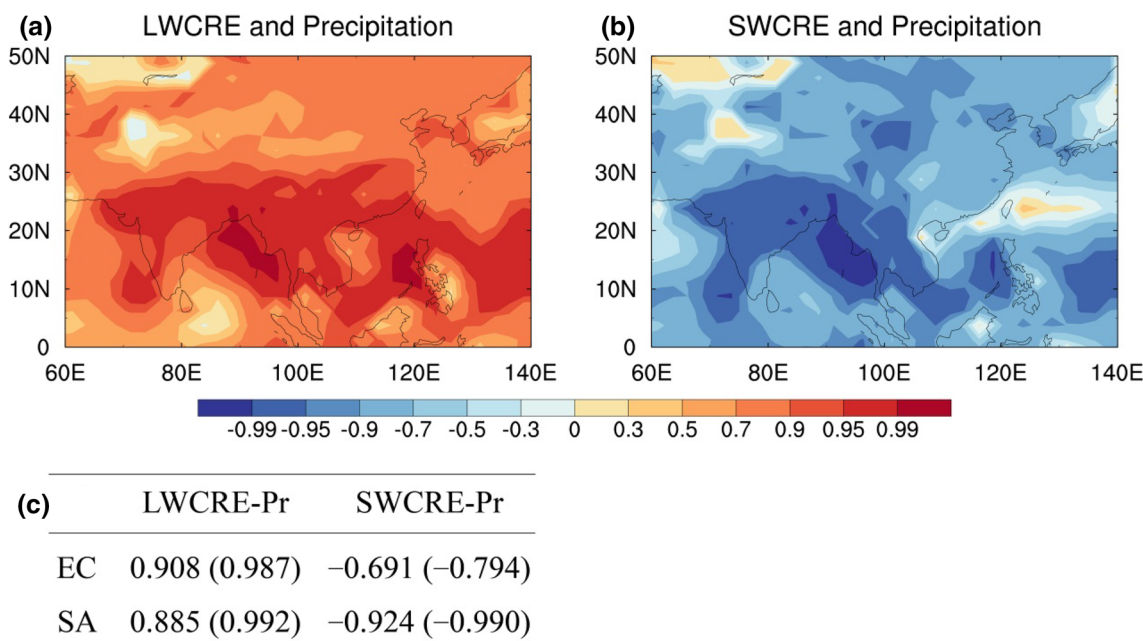


**Fig. 11** Local correlation coefficients between climatological monthly **a** LWCRE and precipitation, and **b** SWCRE and precipitation for the period 2001–2014. **c** Their regional averaged values over EC and SA, and (in parentheses) the correlations of their regional mean values

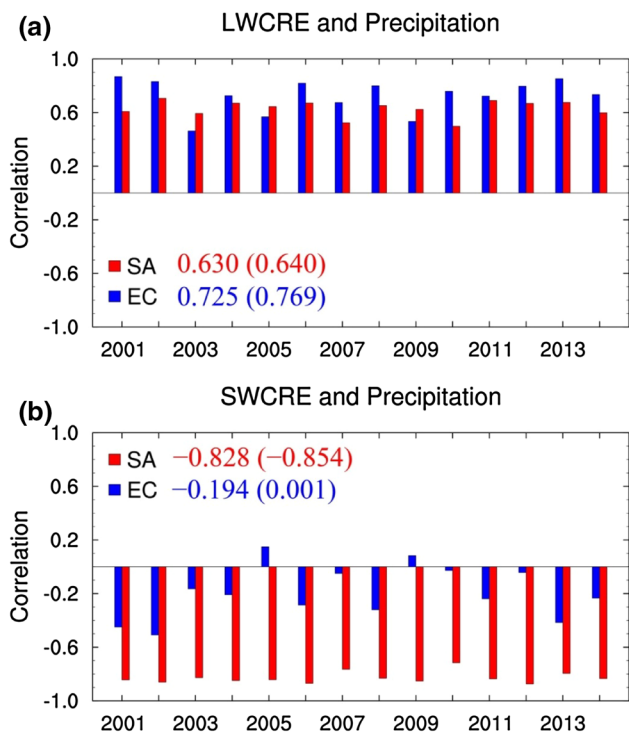


**Fig. 12** Time series of spatial correlation coefficients between **a** LWCRE and precipitation, and **b** SWCRE and precipitation over EC and SA in summer (JJA) for the period 2001–2014. Arithmetic mean values are given for EC (blue) and SA (red), as well as (in parentheses) the correlations of their climatological summer mean values

cloud height and cloud top temperature, which is mainly controlled by the atmospheric thermodynamic condition concurrent with the precipitation intensity over the AMR (Wang 2006). Hence, LWCRE is closely linked to summer precipitation over EC and SA. The intensity of correlation between SWCRE and precipitation depends on cloud types, resulting cloud properties and precipitation. Most of SA belongs to tropics (Sikka and Gadgil 1980), frequent convective systems exist (Luo et al. 2011; Romatschke and Houze 2011) and corresponding clouds are usually large, with high cloud top, large cloud water content and optical depth (Rajeevan and Srinivasan 2000; Rajeevan et al. 2013). In this case, clouds give rise to not only strong precipitation (Fig. 3b, j) but also strong SWCRE (Fig. 2d). Thus, at much degree, summer precipitation corresponds well to SWCRE over SA. Unlike SA, EC lies in the subtropics and its precipitation processes are diverse and complicated (Tao and Chen 1987; Zhu et al. 2007). Summer precipitation processes over EC are not always accompanied by deep convective clouds with large cloud water content and optical depth. For example, it is quite clear in Figs. 6 and 9, vertical motion (convection proxy) and high cloud fraction in summer are larger over SA than over EC. As a result, the physical relationship between SWCRE and precipitation is more complicated over EC and their correlation is then much lower than that over SA (Figs. 11b, 12b). Above-mentioned results show that the difference in the correlation between SWCRE and precipitation over EC and SA probably

arises from their different precipitation-related cloud types and vertical structure during summer.

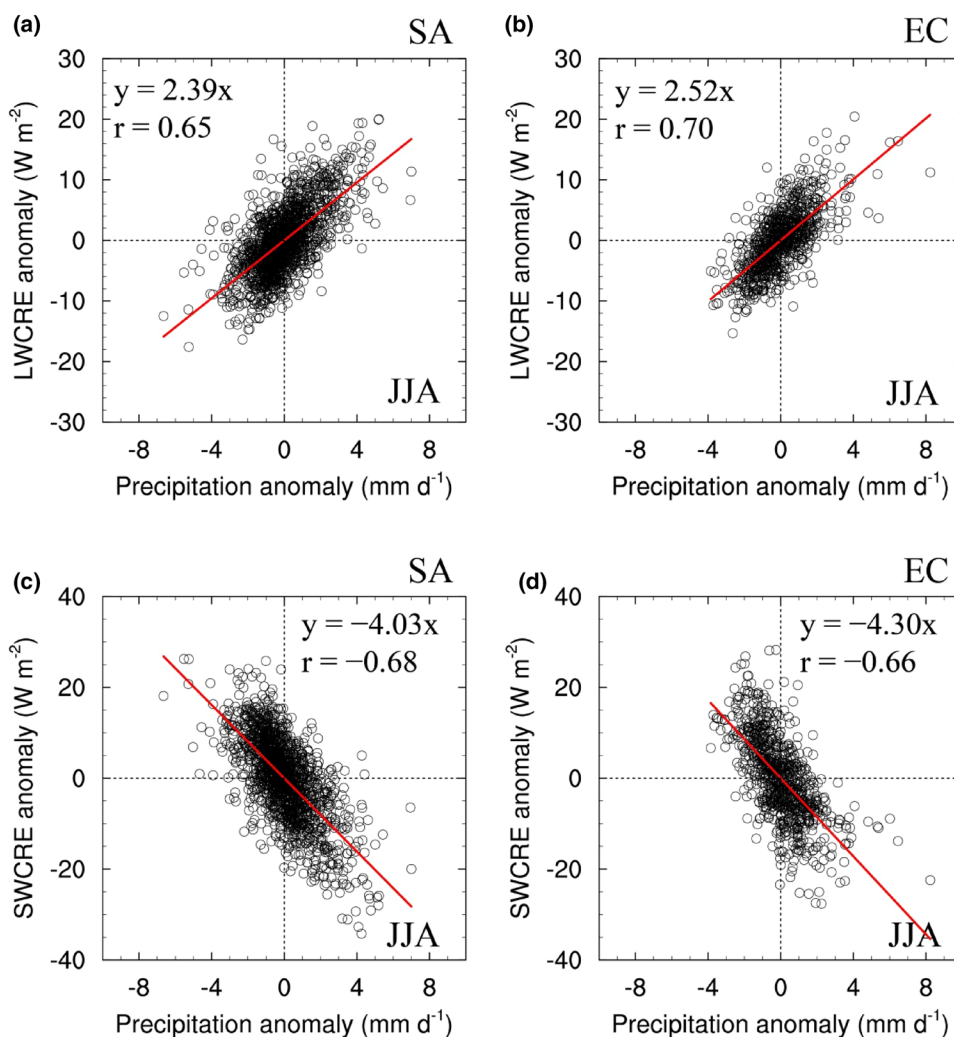
In addition to the effects of climatological mean precipitation on CREs, the relationships between anomalies of inter-annual precipitation and CREs are also examined in summer. As shown in Fig. 13, most positive precipitation anomalies correspond to positive LWCRE (negative SWCRE) over the two sub-AMR regions. For example, the CC over SA is up to 0.65 ( $-0.68$ ) for LWCRE (SWCRE) at the 99% confidence level and the corresponding value is 0.70 ( $-0.66$ ) over EC, indicating heavier precipitation favors stronger CREs. Summer precipitation over the AMR is usually accompanied by active precipitation clouds with high cloud top and a complicated vertical distribution, which readily lead to larger LWCRE and SWCRE.

## 6 Conclusions and discussion

In this study, the seasonal characteristics of TOA CREs and their relationships with column CFs and precipitation over the AMR are investigated using satellite and reanalysis datasets.

The characteristics are found to exhibit remarkable seasonal variations, with key differences between EC and SA. Over SA, seasonal variations of LWCRE and SWCRE are more apparent and in phase, with the maxima in summer and minima in winter; in summer, the centers of LWCRE and SWCRE coincide with those of precipitation. The regional annual mean NCRE over SA is relatively weak because LWCRE significantly compensates SWCRE. Over EC, although the strongest TCF and CREs occur in summer, large LCF and strong SWCRE also appear in winter and persist into summer. The CREs over EC are dominated by strong SWCRE with an annual mean value of up to  $-70 \text{ W m}^{-2}$ , leading to a large NCRE ( $> -40 \text{ W m}^{-2}$ ) cooling effect on the regional atmosphere-surface climate.

**Fig. 13** Scatter plots of inter-annual precipitation anomalies ( $\text{mm d}^{-1}$ ) versus inter-annual CRE anomalies ( $\text{W m}^{-2}$ ) in summer for the period 2001–2014. **a, c** Are for LWCRE and SWCRE over SA, respectively. **b, d** Are over EC. Each circle indicates the summer anomalies of precipitation and CRE at one grid box ( $1^\circ \times 1^\circ$ ) in EC or SA domains. The summer anomaly is the difference between the summer average at each year and the corresponding 2001–2014 mean. Linear correlation coefficients and regression lines (*red*) are shown in each sub-plot. Linear correlation coefficients are at a 99% confidence level



Lower air temperature and higher aerosol loading in winter favor an increase in liquid cloud water content, and a decrease in cloud particle sizes, intensifying the regional cloud albedo effect over EC. Thus, a combination of cloud macro- and micro-physical properties results in the largest TOA albedo ( $>0.5$ ) and SWCRE normalized by incident solar radiation over EC occurring in winter. Moreover, the seasonal amplitudes of TCF and SWCRE variations over EC are obviously weaker than over SA.

The results further show that the differences in TOA CREs over EC and SA are closely related to their CFs and precipitation. Over SA, HCF is predominant; LWCRE and SWCRE have good linear correlations with both TCF and HCF. Over EC, there is apparent low- and middle-level ascending motion and plenty of LCF from winter onwards and SWCRE has a relatively strong relationship with LCF in cold months. With the coming of summer monsoon, TCF and HCF increase significantly and the vertical distribution of clouds becomes more complicated over the AMR. As a result, relationships between CREs and CFs weaken. In addition, our results show that the annual cycles of CREs over SA are consistent with that of precipitation, and their spatial patterns have a good correspondence, meaning that seasonal variations of CREs over SA are mainly driven by the monsoon circulation. Over EC, LWCRE is also closely related to precipitation, but SWCRE is still strongly affected by local cloud properties and shows considerable regional differences.

This study indicates that CREs have close relationships with the predominant column CFs over the AMR, especially in cold months. Thus, to simulate well CREs over the AMR, climate models should be able to capture the properties and structures of the main cloud types. In addition to stratus clouds caused by the TP dynamical and thermal forcing, our analysis further suggests that local cloud micro-physical properties, such as cloud droplet radius, also contribute to the large SWCRE over EC. Previous researches have shown that heavy aerosol loading in EC very likely alters cloud micro-properties, such as number concentration and particle size, and then influences cloud effects on the regional climate (Bennartz et al. 2011; Tao et al. 2012). Hence, cloud micro-physics related to aerosols should also be further investigated to reveal winter CREs characteristics over EC. Moreover, cloud and precipitation processes over the AMR become more complicated in summer. Understanding summer cloud properties associated with precipitation, such as cloud vertical distributions and precipitation-producing systems over the AMR are therefore crucial, as suggested by Luo et al. (2013) and Ravi et al. (2015). Due to limited observations, our study has focused on TOA radiation, CREs, column CFs and total precipitation. To conduct an in-depth study of the spatio-temporal characteristics of CREs and their associations

with precipitation, multi-sources observations including ground and satellite-based datasets are needed to provide more information about cloud properties, particularly for cloud micro-properties and their vertical profiles, and precipitation details. Further climate simulation is also required for quantitatively understanding CREs and relevant influencing processes.

**Acknowledgements** This research was jointly supported by the National Basic Research Program of China (2013CB955803 and 2014CB953902), the National Science Foundation of China (41505130, 41375087 and 91537103), the Chinese Academy of Sciences Ocean Project (XDA11010402), the Third Tibetan Plateau Scientific Experiment (GYHY201406001) and a grant (to SUNYA) from the Office of Sciences (BER), U.S. DOE. CERES-MODIS cloud properties and CERES EBAF products used in this study are produced by the NASA CERES Team, available at <http://ceres.larc.nasa.gov>.

## References

- Adler RF, Huffman GJ, Chang A, Ferraro R, Xie P, Janowiak J, Rudolf B, Schneider U, Curtis S, Bolvin D, Gruber A, Susskind J, Arkin P (2003) The Version 2 Global Precipitation Climatology Project (GPCP) Monthly Precipitation Analysis (1979–Present). *J Hydrometeorol* 4:1147–1167
- Albrecht BA (1989) Aerosols, cloud microphysics, and fractional cloudiness. *Science* 245:1227–1230
- Austin RT, Heymsfield AJ, Stephens GL (2009) Retrieval of ice cloud microphysical parameters using the CloudSat millimeter-wave radar and temperature. *J Geophys Res* 114:D00A23. doi:10.1029/2008JD010049
- Bennartz R, Fan J, Rausch J, Leung LR, Heidinger AK (2011) Pollution from China increases cloud droplet number, suppresses rain over the East China Sea. *Geophys Res Lett* 38:L09704. doi:10.1029/2011GL047235
- Bony S, Lau KM, Sud YC (1997) Sea surface temperature and large-scale circulation influences on tropical greenhouse effect and cloud radiative forcing. *J Clim* 10:2055–2077
- Bony S, Colman R, Kattsov VM et al (2006) How well do we understand and evaluate climate change feedback processes? *J Clim* 19:3445–3482
- Boo K-O, Martin G, Sellar A, Senior C, Byun Y-H (2011) Evaluating the East Asian monsoon simulation in climate models. *J Geophys Res* 116. doi:10.1029/2010jd014737
- Boucher O, Randall D, Artaxo P et al (2013) Clouds and aerosols. In: Stocker et al (ed) *Climate Change 2013: The Physical Science Basis*. Contribution of Working Group I to the Fifth Assessment Report of the Intergovernmental Panel on Climate Change. Cambridge University, Cambridge and New York, pp 571–658
- Cesana G, Chepfer H (2012) How well do climate models simulate cloud vertical structure? A comparison between CALIPSO-GOCCP satellite observations and CMIP5 models. *Geophys Res Lett* 39:L20803. doi:10.1029/2012GL053153
- Cess RD, Potter GL, Blanchet JP et al (1990) Intercomparison and interpretation of climate feedback processes in 19 atmospheric general circulation models. *J Geophys Res* 95(D10):16601–16615. doi:10.1029/JD095iD10p16601
- Chen B, Liu X (2005) Seasonal migration of cirrus clouds over the Asian Monsoon regions and the Tibetan Plateau measured from MODIS/Terra. *Geophys Res Lett* 32:L01804. doi:10.1029/2004GL020868

- Chepfer H, Bony S, Winker D, Cesana G, Dufresne J, Minnis P, Stubenrauch C, Zeng S (2010) The GCM-Oriented CALIPSO Cloud Product (CALIPSO-GOCCP). *J Geophys Res* 115:D00H16. doi:[10.1029/2009JD012251](https://doi.org/10.1029/2009JD012251)
- Clement AC, Burgman R, Norris JR (2009) Observational and model evidence for positive low-level cloud feedback. *Science* 325:460–464
- Dee DP, Uppala SM, Simmons AJ et al. (2011) The ERA-Interim reanalysis: Configuration and performance of the data assimilation system. *Quart J Roy Meteor Soc* 137:553–597
- Ding Y (2007) The variability of the Asian summer monsoon. *J Meteorol Soc Jpn* 85B:21–54
- Ding Y, Chan JC (2005) The East Asian summer monsoon: an overview. *Meteorol Atmos Phys* 89(1–4):117–142
- Doelling DR, Loeb NG, Keyes DF, Nordeen ML, Morstad D, Nguyen C, Wielicki BA, Young DF, Sun M (2013) Geostationary enhanced temporal interpolation for CERES flux products. *J Atmos Ocean Technol* 30:1072–1090
- Dolinar EK, Dong XQ, Xi BK, Jiang JH, Sui H (2015) Evaluation of CMIP5 simulated clouds and TOA radiation budgets using NASA satellite observations. *Clim Dyn* 44(7–8):2229–2247
- Flato G, Marotzke J, Abiodun B et al (2013) Evaluation of Climate Models. In: Stocker et al (ed) *Climate Change 2013: The Physical Science Basis*. Contribution of Working Group I to the Fifth Assessment Report of the Intergovernmental Panel on Climate Change. Cambridge University, Cambridge and New York, pp 571–658
- Guo Z, Zhou TJ (2015) Seasonal variation and physical properties of the cloud system over southeastern China derived from CloudSat products. *Adv Atmos Sci* 32(5): 659–670
- Hartman DL, Moy LA, Fu Q (2001) Tropical convection and the energy balance at the top of the atmosphere. *J Clim* 14:4495–4511
- Hartmann DL, Ockert-Bell ME, Michelson ML (1992) The effect of cloud type on earth's energy balance: Global analysis. *J Clim* 5:1281–1304
- Huffman GJ, Adler RF, Bolvin DT, Gu G (2009) Improving the global precipitation record: GPCP Version 2.1. *Geophys Res Lett* 36:L17808. doi:[10.1029/2009GL040000](https://doi.org/10.1029/2009GL040000)
- Jiang JH, Su H, Zhai C, Perun VS, Genio AD, Nazarenko LS, Donner LJ, Horowitz L, Seman C, Cole J (2012) Evaluation of cloud and water vapor simulations in CMIP5 climate models using NASA “A-Train” satellite observations. *J Geophys Res* 117:D14105. doi:[10.1029/2011JD017237](https://doi.org/10.1029/2011JD017237)
- Kiehl JT (1994) On the observed near cancellation between longwave and shortwave cloud forcing in tropical regions. *J Clim* 7:559–565
- L'Ecuyer TS, Beaudoin HK, Rodell M et al (2015) The observed state of the energy budget in the early twenty-first century. *J Clim* 28:8319–8346
- Li Y, Gu H (2006) Relationship between middle stratiform clouds and large scale circulation over eastern China. *Geophys Res Lett* 33:L09706. doi:[10.1029/2005GL025615](https://doi.org/10.1029/2005GL025615)
- Li J, Liu Y, Wu G (2009) Cloud radiative forcing in Asian monsoon region simulated by IPCC AR4 AMIP models. *Adv Atmos Sci* 26:923–939
- Li J-L, Waliser DE, Stephens G et al (2013) Characterizing and understanding radiation budget biases in CMIP3/CMIP5 GCMs, contemporary GCM, and reanalysis. *J Geophys Res* 118:8166–8184. doi:[10.1002/jgrd.50378](https://doi.org/10.1002/jgrd.50378)
- Liu J, Li Z, Zheng Y, Chiu C, Zhao F, Li C, Cribb M (2013) Cloud optical and microphysical properties derived from ground-based remote sensing over a site in the Yangtze Delta Region. *J Geophys Res Atmos*, doi:[10.1002/jgrd.50648](https://doi.org/10.1002/jgrd.50648)
- Loeb NG, Wielicki BA, Doelling DR, Smith GL, Keyes DF, Kato S, Manalo-Smith N, Wong T (2009) Toward optimal closure of the Earth's top-of-atmosphere radiation budget. *J Clim* 22:748–766
- Loeb NG, Lyman JM, Johnson GC, Allan RP, Doelling DR, Wong T, Soden BJ, Stephens GL (2012a) Observed changes in top-of-the-atmosphere radiation and upper-ocean heating consistent within uncertainty. *Nat Geosci* 5:110–113. doi:[10.1038/NNGEO1375](https://doi.org/10.1038/NNGEO1375)
- Loeb NG, Lyman JM, Johnson GC, Allan RP, Doelling DR, Wong T, Soden BJ, and Stephens GL (2012b) Observed changes in top-of-the-atmosphere radiation and upper-ocean heating consistent within uncertainty. *Nat Geosci* 5(2):110–113
- Luo Y, Zhang R, Wang H (2009) Comparing occurrences and vertical structures of hydrometeors between eastern China and the Indian monsoon region using CloudSat/CALIPSO data. *J Clim* 22:1052–1064
- Luo Y, Zhang R, Qian W, Luo Z, Hu X (2011) Intercomparison of deep convection over the Tibetan Plateau–Asian monsoon region and subtropical North America in boreal summer using CloudSat/CALIPSO data. *J Clim* 24:2164–2177
- Luo Y, Wang H, Zhang R, Qian W, Luo Z (2013) Comparison of rainfall characteristics and convective properties of monsoon precipitation systems over South China and Yangtze-and-Huai River Basin. *J Clim* 26:110–132
- Mace GG, Zhang Q, Vaughan M, Marchand R, Stephens G, Trepte C, Winker D (2009) A description of hydrometeor layer occurrence statistics derived from the first year of merged Cloudsat and CALIPSO data. *J Geophys Res* 114:D00A26. doi:[10.1029/2007JD009755](https://doi.org/10.1029/2007JD009755)
- Minnis P, Sun-Mack S, Young DF, Heck PW, Garber DP, Chen Y et al (2011a) CERES Edition-2 cloud property retrievals using TRMM VIRS and Terra and Aqua MODIS data, Part I: algorithms. *IEEE Trans Geosci Remote Sens* 49:4374–4400
- Minnis P, Sun-Mack S, Chen Y, Khaiyer MM, Yi Y, Ayers JK et al (2011b) CERES Edition-2 cloud property retrievals using TRMM VIRS and Terra and Aqua MODIS data, Part II: examples of average results and comparisons with other data. *IEEE Trans Geosci Remote Sens* 49:4401–4430
- Rajeevan M, Srinivasan J (2000) Net Cloud Radiative Forcing at the Top of the Atmosphere in the Asian Monsoon Region. *J Clim* 13:650–657
- Rajeevan M, Nanjundiah R (2010) Coupled model simulations of twentieth century climate of the Indian summer monsoon. In: *Current trends in science*, Indian Academy of Sciences. Platinum Jubilee Publication, Bangalore, pp 537–567
- Rajeevan M, Rohini P, Niranjan Kumar K, Srinivasan J, Unnikrishnan CK (2013) A study of vertical cloud structure of the Indian summer monsoon using CloudSat data. *Clim Dyn* 40:637–650
- Ramanathan V, Cess RD, Harrison EF, Minnis P, Barkstrom BR, Ahmad E, Hartmann D (1989) Cloud-radiative forcing and climate: Results from the earth radiation budget experiment. *Science* 243:57–63
- Randall DA et al (2007) Climate models and their evaluation. In: S. Solomon et al (eds.) *Climate change 2007: the physical science basis* Cambridge University, Cambridge
- Ravi KV, Rajeevan M, Gadhavi H, Rao SVB, Jayaraman A (2015) Role of vertical structure of cloud microphysical properties on cloud radiative forcing over the Asian monsoon region. *Clim Dyn*. doi:[10.1007/s00382-015-2542-0](https://doi.org/10.1007/s00382-015-2542-0)
- Rogers RR and Yau MK (1989) *A Short Course in Cloud Physics*. Butterworth-Heinemann, p 304
- Romatschke U, Houze RA Jr (2011) Characteristics of precipitating convective systems in the South Asian monsoon. *J Hydrometeorol* 12:157–180
- Rossow WB, Schiffer RA (1999) Advances in understanding clouds from ISCCP. *Bull Am Meteorol Soc* 80:2261–2288

- Sikka D, Gadgil S (1980) On the maximum cloud zone and the ITCZ over Indian, longitudes during the southwest monsoon. *Mon Weather Rev* 108:1840–1853
- Simmons AJ, Willett KM, Jones PD, et al. (2010) Low frequency variations in surface atmospheric humidity, temperature, and precipitation: Inferences from reanalyses and monthly gridded observational data sets. *J Geophys Res* 115, doi:[10.1029/2009JD012442](https://doi.org/10.1029/2009JD012442)
- Simmons AJ, Poli P, Dee DP, Berrisford P, Hersbach H, Kobayashib S, Peubey C (2014) Estimating low-frequency variability and trends in atmospheric temperature using ERA-Interim. *Q J R Meteorol Soc* 140:329–353. doi:[10.1002/qj.2317](https://doi.org/10.1002/qj.2317)
- Stephens GL (2005) Cloud feedbacks in the climate system: a critical review. *J Clim* 18(2):237–273
- Stevens B, Bony S (2013) What are climate models missing? *Science* 340:1053–1054. doi:[10.1126/science.1237554](https://doi.org/10.1126/science.1237554)
- Stubenrauch C, Rossow W, Kinne S, Ackerman S, Cesana G, Chefer H, Di Girolamo L, Getzewich B, Guignard A, Heidinger A (2013) Assessment of global cloud datasets from satellites: Project and database initiated by the GEWEX radiation panel. *Bull Am Meteorol Soc* 94(7):1031–1049
- Tao SY, Chen LX (1987) A review of recent research on the East Asian summer monsoon in China. In: *Meteorology Monsoon* (ed.) CP Chang, TN Krishnamurti. Oxford Univ. Press, Oxford, pp 60–92
- Tao WK, Chen JP, Li Z, Wang C, Zhang C (2012) Impact of aerosols on convective clouds and precipitation. *Rev Geophys* 50:RG2001. doi:[10.1029/2011RG000369](https://doi.org/10.1029/2011RG000369)
- Trenberth KE, Fasullo JT, Kiehl J (2009) Earth's global energy budget. *Bull Am Meteorol Soc* 90(3):311–323. doi:[10.1175/2008bams2634.1](https://doi.org/10.1175/2008bams2634.1)
- Twomey SA (1977) The influence of pollution on the shortwave albedo of clouds. *J Atmos Sci* 34:1149–1152
- Wang B (2006) *The Asian Monsoon*. Springer/Praxis, New York, p 450
- Wang WC, Gong W, Kau WS, Chen CT, Hsu HH, Tu CH (2004) Characteristics of cloud radiation forcing over East China. *J Clim* 17(4):845–853
- Wang F, Yang S, Wu T (2014) Radiation budget biases in AMIP5 models over the East Asian monsoon region. *J Geophys Res Atmos* 119:13400–13426. doi:[10.1002/2014JD022243](https://doi.org/10.1002/2014JD022243)
- Webster PJ, Magana VO, Palmer TN, Shukla J, Tomas RA, Yanai M, Yasunari T (1998) Monsoons: processes, predictability, and the prospects for prediction. *J Geophys Res* 103(C7):14451–14510
- Wild M, Folini D, Schar C, Loeb N, Dutton EG, Langlo GK (2013) The global energy balance from a surface perspective. *Clim Dyn* 40(11–12):3107–3134
- Wood R, Bretherton CS (2006) On the relationship between stratiform low cloud cover and lower-tropospheric stability. *J Clim* 19:6425–6432
- Wu G, Liu Y, Wang T, Wan R, Liu X, Li W, Wang Z, Zhang Q, Duan A, Liang XY (2007) The influence of mechanical and thermal forcing by the Tibetan Plateau on Asian climate. *J Hydrometeorol* 8:770–789
- Yin P, Gruber A, Arkin P (2004) Comparison of the GPCP and CMAP merged gauge-satellite monthly precipitation products for the period 1979–2001. *J Hydrometeorol* 5:1207–1222
- Yu R, Yu Y, Zhang M (2001) Comparing cloud radiative properties between the eastern China and the Indian monsoon region. *Adv Atmos Sci* 18(6):1090–1102
- Yu R, Wang B, Zhou T (2004) Climate effects of the deep continental stratus clouds generated by the Tibetan Plateau. *J Clim* 17(13):2702–2713
- Zhang Y, Yu R, Li J, Yuan W, Zhang M (2013) Dynamic and thermodynamic relations of distinctive stratus clouds on the lee side of the Tibetan Plateau in the cold season. *J Clim* 26(21):8378–8391
- Zhu QG, Lin JR, Shou SW, Tang DS (2007) *The weather principles and methods*. Meteorological Press, Beijing, p 649